ACS APPLIED MATERIALS & INTERFACES

Letter

www.acsami.org

Air-Stable, Solution-Processed Oxide p–n Heterojunction Ultraviolet Photodetector

Do Young Kim,‡ Jiho Ryu,‡ Jesse Manders, Jaewoong Lee, and Franky So*

Department of Materials Science and Engineering, University of Florida, Gainesville, Florida 32611, United States

ABSTRACT: Air-stable solution processed all-inorganic p–n heterojunction ultraviolet photodetector is fabricated with a high gain (EQE, 25 300%). Solution-processed NiO and ZnO films are used as p-type and n-type ultraviolet sensitizing materials, respectively. The high gain in the detector is due to the interfacial trap-induced charge injection that occurs at the ITO/NiO interface by photogenerated holes trapped in the NiO film. The gain of the detector is controlled by the post-annealing temperature of the solution-processed NiO films, which are studied by X-ray photoelectron spectroscopy (XPS).

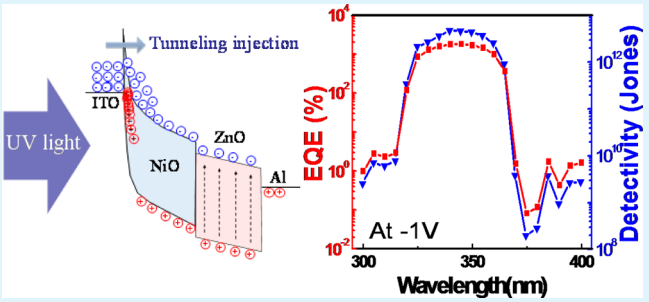

KEYWORDS: *photodetector, ultraviolet, NiO, ZnO, solution process*

INTRODUCTION

Ultraviolet (UV) photodetectors are important devices with applications such as solar-blind detectors, biosensors, and ozone detectors.[1,2] Conventional UV photodetectors are based on wide-gap inorganic semiconductors such as SiC, GaN, and diamond which require expensive vacuum processing. Recently, solution-processed inorganic nano-materials such as PbS quantum dots (QDs) and ZnO nanoparticles (NPs) have attracted a great deal of attention because of their potential for low-cost photodetectors to be used in a wide spectral range from the near-infrared to the UV region.[3,4] Recently, solution-processed ZnO NPs UV photoconductors showed a high responsivity up to 61 A/W.[3] However, ZnO photoconductors with a lateral architecture leads to a high driving voltage (>100 V) due to the large spacing between electrodes. More recently, solution-processed hybrid organic–inorganic UV photodetectors based on a blend of ZnO NPs and a semiconducting polymer with a high responsivity (1000 A/W) have been reported.[5] The high gain (EQE > 340 000%) in these hybrid detectors was attributed to electron-trapped-induced charge injection in the ZnO NPs. These photodetectors are thin film devices with a thickness less than 1 μm, thus leading to a low operating voltage (< 10 V). Organic charge blocking layers in these hybrid detectors are inserted between the electrodes and the active layer to reduce the dark current due to the high energy barriers from the electrodes to the active layer. However, organic materials might not be stable under ambient conditions.[6−8] Therefore, it is desirable to fabricate devices using solution-processable inorganic materials. In this work, we have successfully demonstrated air-stable, high-gain, solution-processed all-inorganic heterojunction UV photodetectors.

RESULTS AND DISCUSSION

The structure of our photodetector is shown in Figure 1a. The device consists of a p-type NiO layer, an n-type ZnO layer, an

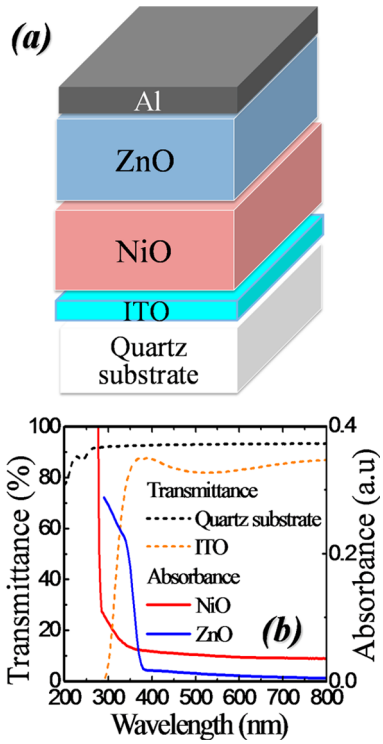

Figure 1. (a) Schematic cross-section view of solution processed UV photodetector and (b) absorbance spectra of oxide layers (NiO, ZnO) and transmittance spectra of ITO anode and quartz substrate used in this study.

Received: November 7, 2013
Accepted: January 9, 2014
Published: January 9, 2014

ITO anode, and an Al cathode. NiO has a conduction band edge of 1.8 eV and a valence band edge of 5.5 eV, and ZnO has a conduction band edge of 4.2 eV and a valence band edge of 7.6 eV. Hetero-epitaxially grown NiO/ZnO p−n heterojunction UV detectors have been reported with a responsivity of 0.3 A/W.[9] In this study, NiO/ZnO layers are deposited by solution process as described in the experimental procedure. Figure 1b shows the absorbance spectra of a NiO film and a ZnO film and the transmittance spectra of an ITO anode and a quartz substrate. As shown in the figures, both NiO and ZnO have strong absorption in the ultraviolet part of the spectrum. The NiO film and ZnO film show absorption onsets at 330 nm and 365 nm corresponding to optical bandgaps of 3.7 and 3.4 eV, respectively. Because both materials absorb only in the UV region, the resulting device is completely transparent to the visible light. In fact, the UV cutoff wavelength of the detector is limited to the transparency of the ITO anode.

Figure 2a shows the current−voltage (J−V) characteristics of a solution processed UV photodetector measured in the dark and under UV illumination at λ = 350 nm with a light intensity of 45 μW/cm^2. To fabricate such a device, a NiO film was first spin-coated on an ITO coated substrate and annealed at 350 °C for 40 min and subsequently a ZnO film was spin-coated on top of the NiO film followed by annealing at 100 °C for 10 min. The resulting UV detector exhibits typical rectifying characteristics of a p−n junction diode with a rectification ratio of ∼5 × 10^2 (± 1 V). Under UV illumination, the diode shows a strong photocurrent response. To obtain the responsivity (R) of the photodiode, we measured the external quantum efficiency (EQE) using a lock-in amplifier, as described in experimental procedure. The results are shown in Figure 2b. At a reverse bias of −1 V, the EQE exceeds 100% at ∼365 nm and it reaches a maximum value of 1800% at λ = 350 nm. The EQE spectrum is consistent with the absorption spectrum of the ZnO film. The responsivity reaches a maximum of 10.2 A/W at λ = 350 nm under a bias voltage at −1 V. Here, the sensitivity of the detector is only in the UV region, demonstrating its applications for UV photodetectors.

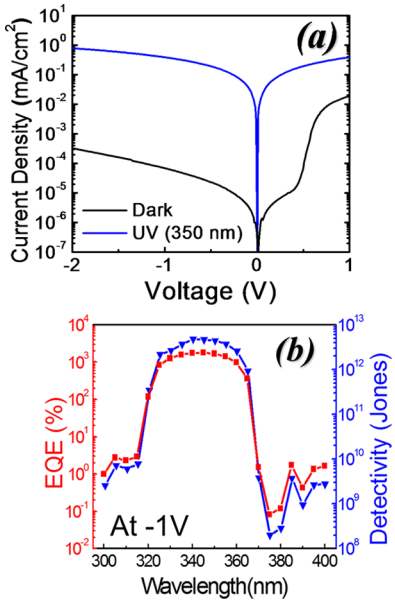

Figure 2. (a) I−V characteristics under dark and under UV illumination (350 nm, 45 μW/cm^2) and (b) the EQE and the detectivity values as function of wavelength under reverse bias in the UV photodetector.

The detectivity (D^*) of a photodetector is given by the following expression

$$D^* = R(A\Delta f)^{1/2}/i_n \quad (1)$$

where R is the responsivity, A is the device area, Δf is the bandwidth and i_n is the noise current. Assuming that shot noise due to the dark current is a major contribution in the total noise current of the photodetector, the detectivity is then given by the following expression[10]

$$D^* = R/(2qJ_d)^{1/2} = (J_{ph}/L_{light})(2qJ_d)^{1/2} \quad (2)$$

where R is the responsivity, q is the electron charge, J_d is the dark current, J_{ph} is the photocurrent, and L_{light} is the incident power density. This assumption has been demonstrated to be valid for a similar UV detector using a polymer:ZnO nanocomposite.[5] The detectivity is then calculated using eq 2 and the results are shown in Figure 2b. The detectivity value exceeds 1 × 10^{12} Jones from 320 nm to 365 nm and it reaches a maximum of 4.66 × 10^{12} Jones at λ = 350 nm under a bias of −1 V.

The gain in photodetectors with a similar photodiode structure has been attributed to interfacial trap-induced charge injection.[5,11] To understand the physical origin of gain in these UV detectors, we studied the composition of the solution-derived NiO films using X-ray photoelectron spectroscopy (XPS). Figure 3a shows the XPS spectrum for the Ni 2p$_{3/2}$ state, which can be separated into three peaks. First, the peak centered at a binding energy of 853.4 eV corresponds to Ni^{2+} in the standard Ni−O octahedral bonding configuration.[12,13] Second, the broad peak centered at 860 eV has been attributed to as the shakeup peak in the NiO structure.[12,13] Finally, the peak centered at 855.2 eV corresponds to the Ni^{2+} vacancy-induced Ni^{3+} ions in Ni_2O_3 or nickel hydroxides (Ni-

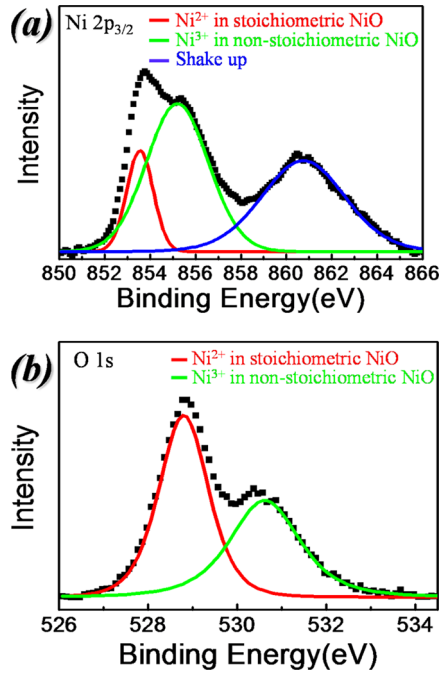

Figure 3. XPS spectra for (a) the Ni 2p$_{3/2}$ state and (b) O 1s state in the NiO film with the post annealing temperature of 350 °C.

dx.doi.org/10.1021/am4050019 | ACS Appl. Mater. Interfaces 2014, 6, 1370−1374

$(OH)_2$).[12−14] Figure 3b shows the XPS spectrum for the O 1s state, which can be separated into two distinct peaks. The peak centered at 528.9 eV confirms the Ni−O octahedral bonding in NiO.[12,13] The peak at 531.0 eV is indicative of the presence of Ni_2O_3 or $Ni(OH)_2$.[13−15] Therefore, the XPS data indicate that the NiO film is composed of Ni_2O_3 and $Ni(OH)_2$ as well as NiO. It has been reported that the activation energy of the electrical conduction, which exhibit the energetic depth of an electrical trap state within a forbidden energy gap between the valence band maximum and the conduction band minimum of a semiconductor, in solution-processed NiO thin films increases with increasing content of Ni_2O_3 and $Ni(OH)_2$, thus indicating that the portion of Ni_2O_3 and $Ni(OH)_2$ behaves as an electrical trap site in the NiO film.[16] Therefore, the gain observed in our photodiode is possibly due to interfacial trap-controlled charge injection.

To understand the correlation of the detector gain mechanism and the nature of the defects presence in the NiO films, we fabricated detectors with three different NiO post annealing temperatures of 270, 350, and 540 °C. The EQEs and the detectivities of the resulting devices are presented in Figure 4a. Both the EQE and the detectivity of the detector increase with decreasing post annealing temperature. Specifically, the device annealed at 270 °C shows an EQE up to 25 300% and a detectivity up to 2×10^{13} Jones, whereas the detector annealed at 540 °C shows an EQE of 189% and a detectivity of 1×10^{12} Jones. On the other hand, from the XPS data, the non-stoichiometric portion of the NiO film decreases with increasing post annealing temperature as shown in Figure 4b. The decreased nonstoichiometric NiO with increasing annealing temperature is strongly correlated with the decrease in EQE and detectivity in the UV detector with increased NiO annealing temperature, indicating that the defects due to the non-stoichiometric NiO present in the film is strongly related to the gain mechanism of the detector. Detectors with different ZnO post annealing temperatures were also fabricated but both the EQE and the detectivity of the detector were independent on the ZnO post annealing temperature. Therefore, the gain in detectors is due to the trap sites in not the ZnO film but the NiO film.

To further understand the nature of defects due to non-stoichiometric NiO, we characterized the temporal response of the UV detectors with different NiO annealing temperatures by UV pulses generated using a shutter. It is expected that the speed of the detector with a larger gain should be slower because of strong carrier trapping.[17] Figure 4c shows the rise time, which is defined as the time changing from 10 to 90% of the peak output value, and the fall time, which is the time changing from 90 to 10% of the peak output value, of the detectors with different NiO annealing temperatures under −1 V. The rise times are 6.5, 1.8, and 0.2 s and the fall times are 4.8, 1.6, and 0.18 s for devices annealed at 270, 350, and 540 °C, respectively It is apparent that the rise and fall times decrease with the increased NiO annealing temperatures, as expected.

Figure 5 shows the schematic energy band diagrams to explain the gain mechanism of our UV photodetector. In the detector with a p−n heterojunction structure under dark and reverse bias condition, the p-type NiO layer blocks electron injection from the ITO anode and the n-type ZnO layer blocks hole injection from the Al cathode effectively as shown in Figure 5a. Under UV illumination and reverse bias as shown in Figure 5b, however, the ZnO layer absorbs incident photons

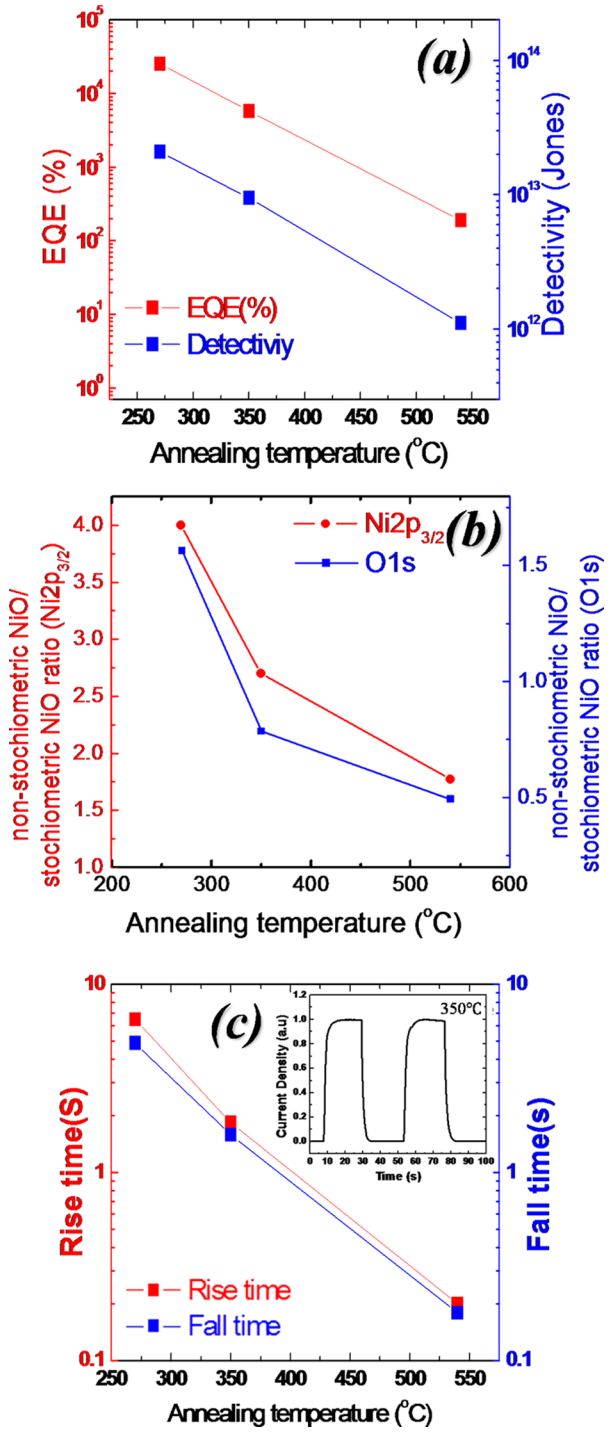

Figure 4. NiO annealing temperature dependence of (a) the EQE and the detectivity, (b) the portion of Ni_2O_3 and $Ni(OH)_2$ in the NiO film, and (c) the response time (rise and fall times under −1 V).

and generates electron−hole pairs. Whereas the photogenerated electrons are transported through the ZnO layer to the Al cathode, the photogenerated holes are transported from the ZnO layer to the NiO layer. Some holes are transported through the NiO layer to the ITO anode but some others are trapped in the defect sites in the NiO film. The trapped holes subsequently shift the valence band edge of the NiO film upwards and align the Fermi energy of the NiO film with that of the ITO anode, resulting in electron tunneling through the barrier at the ITO/NiO interface.

dx.doi.org/10.1021/am4050019 | ACS Appl. Mater. Interfaces 2014, 6, 1370−1374

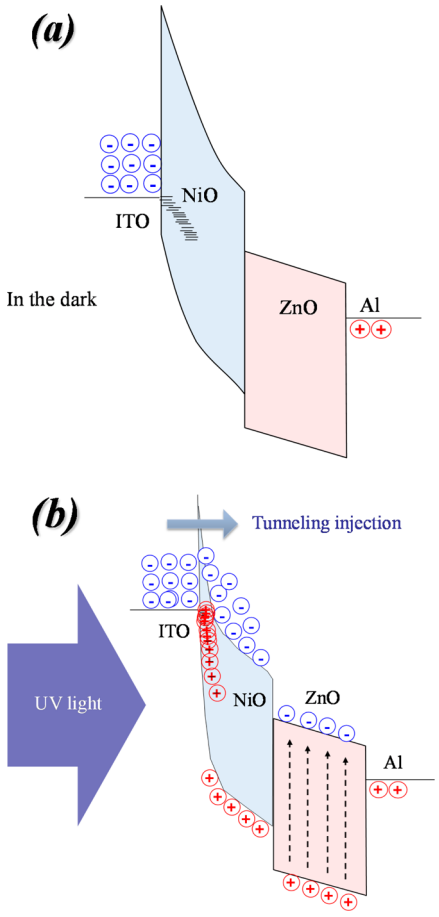

Figure 5. Schematic energy band diagrams of the UV photodetector with gain (a) in the dark and (b) in the UV illumination.

As we mentioned above, the entire all-inorganic UV detector consists of all oxide layers (ITO anode, p-type NiO layer, and n-type ZnO layer) and are expected to have a good air stability. To evaluate the air stability, detectors with three different NiO annealing temperatures are fabricated without any encapsulation and the device performance was monitored during storage in air. Figure 6 shows the shelf life of the EQE and detectivity. As shown in the figure, both the EQE and detectivity are slightly enhanced in all three devices in the first 20 days, indicating that the oxide layers were further stabilized in the atmosphere. The EQE and the detectivity begin to decrease slightly after 20 days but are still higher than the initial values

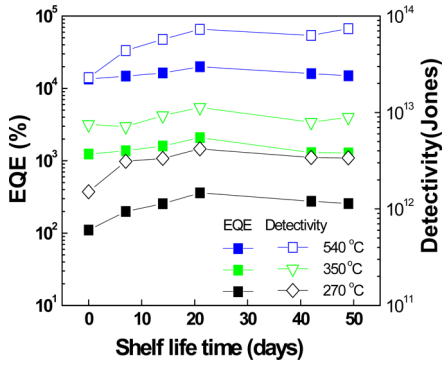

Figure 6. Stability test of the oxide-based solution processed UV photodetector.

even after 50 days. Therefore, the long-term stability of our solution-processed oxide-based detectors is promising.

CONCLUSION

We fabricated solution-processed all-inorganic p−n heterojunction UV photodetectors using NiO and ZnO films as p-type and n-type wide bandgap semiconductors. The UV detectors have a high gain with a long life time. The high gain in the detector is due to interfacial trap-induced charge injection which occurs at the ITO/NiO interface by photogenerated holes trapped in the NiO film. The long shelf life is due to the stability of all oxide layers. These solution-processed oxide p−n heterojunction UV photodetectors have a great potential for replacing conventional vacuum-deposited UV photodetectors for new applications.

EXPERIMENTAL SECTION

NiO Precursor Solution. Nickel acetate tetrahydrate ($Ni(CH_3COO)_2 \bullet 4H_2O$) (Acros Organics) was dissolved in ethanol with monoethanolamine ($NH_2CH_2CH_2OH$) (Sigma-Aldrich) (0.1 mol L^{-1}). The molar ratio of Ni^{2+}: MEA was maintained at 1:1 in solution. Dissolution took place while stirring in a sealed glass vial at 70° C for 4 h. The solution appeared homogeneous and deep green after approximately 40 min.

ZnO NP Synthesis. ZnO NPs ranging from 3 to 5 nm in size were synthesized by a sol−gel process using precursors of zinc acetate and tetramethylammonium hydroxide (TMAH). For a typical process, the ZnO NPs were synthesized by slow dropwise addition of a stoichiometric amount of TMAH dissolved in ethanol (0.55M) to 0.1 M zinc acetate dihydrate dissolved in dimethyl sulfoxide (DMSO), followed by stirring for an hour. After being washed, the ZnO NPs were dissolved in ethanol and stored under ambient conditions. All solutions were filtered with a 0.45 μm filter.

Device Fabrication. Solution-processed p−n heterojunction UV photodetectors were fabricated on quartz substrates. The quartz substrates were first cleaned with acetone and isopropanol in an ultrasonic cleaner and subsequently rinsed with deionized water, and blown dry with N_2 gas. ITO was sputtered on the quartz substrates for 15 minutes, and then treated with UV ozone for 15 minutes. NiO films (130 nm thick) were first spin-coated onto the substrate as a p-type oxide layer and the film was subsequently annealed at 270, 350, and 540 °C for 40 min, respectively. ZnO films (70 nm thick) were spin-coated on the substrates as an n-type oxide layer and the film was annealed at 100 °C for 10 min. Finally, the device was finished by thermally evaporating 100 nm of Al at a rate of 1 Å/s as a cathode. The area of the device is 0.04 cm^2.

Device Characterization. The current−voltage (J−V) characteristics of the devices were measured with a Keithley 4200 semiconductor parameter analyzer. The photoresponse measurements were down with the devices irradiated with monochromatic lights from a Newport monochromator using an Oriel solar simulator as a source. The illumination intensity was measured by a calibrated Newport 918D photodiode. To obtain the spectral response of the photodetectors, light from the monochromator was chopped at 400 Hz to modulate the optical signal. The photocurrent response as a function of bias voltage was measured using a Stanford Research System SR810 DSP lock-in amplifier. The spectral response was also used to calculate the spectral detectivity of the devices.

dx.doi.org/10.1021/am4050019 | ACS Appl. Mater. Interfaces 2014, 6, 1370−1374

AUTHOR INFORMATION

Corresponding Author

*E-mail: fso@mse.ufl.edu.

Author Contributions

‡The manuscript was written through contributions of all authors. Authors D.-Y.K. and J.R. contributed equally.

Notes

The authors declare no competing financial interest.

ACKNOWLEDGMENTS

The authors acknowledge Nanoholdings for support of this work.

REFERENCES

(1) Li, W. D.; Chou, S. Y. *Opt. Express* **2010**, *18*, 931−937.
(2) Razeghi, M.; Rogalski, A. *J. Appl. Phys.* **1996**, *79*, 7433−7473.
(3) Jin, Y. Z.; Wang, J. P.; Sun, B. Q.; Blakesley, J. C.; Greenham, N. C. *Nano Lett.* **2008**, *8*, 1649−1653.
(4) Konstantatos, G.; Howard, I.; Fischer, A.; Hoogland, S.; Clifford, J.; Klem, E.; Levina, L.; Sargent, E. H. *Nature* **2006**, *442*, 180−183.
(5) Guo, F.; Yang, B.; Yuan, Y.; Xiao, Z.; Dong, Q.; Bi, Y.; Huang, J. *Nat. Nanotechnol.* **2012**, *7*, 798−802.
(6) So, F.; Kondakov, D. *Adv. Mater.* **2010**, *22*, 3762−3777.
(7) Jorgensen, M.; Norrman, K.; Krebs, F. C. *Sol. Energy Mater. Sol. Cells* **2008**, *92*, 686−714.
(8) Kumar, A.; Devine, R.; Mayberry, C.; Lei, B.; Li, G.; Yang, Y. *Adv. Funct. Mater.* **2010**, *20*, 2729−2736.
(9) Ohta, H.; Kamiya, M.; Kamiya, T.; Hirano, M.; Hosono, H. *Thin Solid Films* **2003**, *445*, 317−321.
(10) Gong, X.; Tong, M.; Xia, Y.; Cai, W.; Moon, J. S.; Cao, Y.; Yu, G.; Shieh, C.; Nilsson, B.; Heeger, A. J. *Science* **2009**, *325*, 1665−1667.
(11) Chen, H.; Lo, M.; Yang, G.; Monbouquette, H.; Yang, Y. *Nat. Nanotechnol.* **2008**, *3*, 543−547.
(12) Kim, K. S.; Winograd, N. *Surf. Sci.* **1974**, *43*, 625−643.
(13) Manders, J. R.; Tsang, S.-W.; Hartel, M. J.; Lai, T.-H.; Chen, S.; Amb, C. M.; Reynolds, J. R.; So, F. *Adv. Funct. Mater.* **2013**, *23*, 2993−3001.
(14) Ratcliff, E. L.; Meyer, J.; Steirer, K. X.; Garcia, A.; Berry, J. J.; Ginley, D. S.; Olson, D. C.; Kahn, A.; Armstrong, N. R. *Chem. Mater.* **2011**, *23*, 4988−5000.
(15) Han, S. Y.; Lee, D. H.; Chang, Y. J.; Ryu, S. O.; Lee, T. J.; Chang, C. H. *J. Electrochem. Soc.* **2006**, *153*, C382−C386.
(16) Soleimanpour, A. M.; Khare, S. V.; Jayatissa, A. H. *ACS Appl. Mater. Interfaces* **2012**, *4*, 4651−4657.
(17) Konstantatos, G.; Levina, L.; Fischer, A.; Sargent, E. H. *Nano Lett.* **2008**, *8*, 1446−1450.